EXTREME MECHANICS
LETTERS

Description of the image

Trapping and attenuating broadband vibroacoustic energy with hyperdamping metamaterials

CrossMark

Ryan L. Harne *, Yu Song, Quanqi Dai

Department of Mechanical and Aerospace Engineering, The Ohio State University, Columbus, OH 43210, USA

ABSTRACT

We introduce a class of engineered metamaterials for the purpose of attenuating and trapping spectrally broadband vibration and acoustic energy. The physical phenomenon realized to effect such wideband energy dissipation performance is termed hyperdamping since it is the consequence of eliminating fundamental stiffness contributions within the material system so as to asymptotically enhance damping properties. A strategically sculpted elastomer topology is geometrically constrained and embedded in a poroelastic matrix to realize the metamaterial platform. Finite element model analyses guide design of the embedded hyperdamping inclusions while experimental studies on dynamic force transmissibility and acoustical absorption coefficient provide conclusive evidence that hyperdamping phenomena facilitate wideband energy dissipation in a lightweight material system that is not subject to the limitations of conventional resonance- or bandgap-based attenuation effects. The hyperdamping metamaterials thus meet the often conflicting performance requirements of real applications where broadband vibrations and noise must be abated using lightweight material solutions.

1. Background, motivation, and new idea

The absorption or attenuation of spectrally broadband vibration and wave energy are goals that have called upon the efforts of researchers spanning diverse engineering and scientific disciplines over the years [1]. While resonant phenomena can facilitate striking vibroacoustic energy trapping [2,3], many scenarios involve wide-band or stochastic energy sources for which broadband energy capture is necessary. Unfortunately, the only assured solution for broadband energy attenuation is to introduce excessive mass between the dynamic energy source and the region/receiver of interest [4], which conflicts with requirements for many applications, such as vehicular systems, where added mass is detrimental to performance and effectiveness. In addition, while input energies may cause vibrations at low frequencies associated with modal oscillations, practical structures transfer the energy to higher frequencies due to joints, friction, and complex geometries [5,6], thus creating a 'noise problem' in a bandwidth most sensitive to humans [6] through inevitable structure–fluid interaction. Although conventional noise control treatments such as lightweight, poroelastic media [7] are well-suited to dampen waves in this mid-to-high frequency range, they are ill-suited to attenuate low frequency vibrations and sound within typical size constraints [8]. As a result, lightweight materials to dampen spectrally broadband vibroacoustic energies are in demand [9].

To address the challenges, researchers are exploring strategically architected material systems that provide elastic and acoustic wave attenuation capabilities not otherwise found in bulk structural materials. Among them, resonant metamaterials and phononic crystals exhibit opportunities to suppress vibration and wave energies due to tuned–mass–damper or bandgap effects [10–12]. Yet, despite the advancements, the energy attenuation properties are reliant upon resonance- or bandgap-related phenomena that are often parameter sensitive and narrowband [13]. In addition, many experimental realizations have been proposed using heavy materials including metals and dense rubbers [11,12,14] which are inadequate solutions in the numerous practical applications where treatment weight is a great penalty.

Building upon these ideas, periodic, elastic metamaterials leveraging instability mechanisms are shown to yield remarkable wave propagation control and energy absorption capabilities due to energy changes associated with transitions among internal topologies [15–17]. On the other hand, these elastic systems are likewise realized by dense materials such as silicones [17] or 3D-printed polymers [18] that are ill-suited for applications where increased treatment density comes at a high cost. Static stresses or exterior displacement constraints may also be needed to achieve the

---

* Corresponding author.
   E-mail address: harne.3@osu.edu (R.L. Harne).

wave tailoring properties through the buckling instability [16,19], which prevents implementing such metamaterials as absorbers of free field acoustic energy, in the operational mode similar to conventional poroelastic foams. In fact, it is well-known that buckling instability-based phenomena can enhance energy dissipation properties [20]. Such anomalous damping is due to a cancellation of the positive and negative stiffnesses, a design condition termed the *elastic stability limit* [21], which eliminates the fundamental natural frequency $\omega_n \rightarrow 0$. The important consequence of the elastic stability limit for this new research is that the damping ratio grows without bound [22–24] according to the classic relation for the fundamental modal damping ratio $\zeta = c/2m\omega_n$ where c and m are the modal damping constant and mass, respectively [25]. Yet, considering these investigations on elastic metamaterials, despite the recent advancements the reliance upon parameter-sensitive resonance-related phenomena, the use of dense materials, and possible need for exterior material constraints make these concepts insufficient solutions for applications demanding lightweight materials for broadband vibration and acoustic energy capture.

With a different material design perspective in mind, other recent studies show that heterogeneous, poroelastic metamaterials can achieve considerable wave and/or vibration energy absorption. For instance, randomly embedding solid, metal inclusions into poroelastic foams improves the low frequency attenuation of the host media [26]. Periodically distributing such inclusions also spawns bandgap phenomena [27] to substantially increase low frequency vibroacoustic energy absorption via "trapped" mode effects [28,29]. On the other hand, such advancements lack the encompassing promise of broadband vibroacoustic energy dissipation in a lightweight system design; instead, these poroelastic metamaterials excel at one or another of the individual performance measures.

By integrating concepts from metamaterials with elastic instabilities and ideas from investigations on heterogeneous poroelastic media, in this research we introduce a new framework of lightweight, hyperdamping metamaterials that interface with the acoustic free field to achieve large vibration and acoustic wave energy attenuation. Fig. 1 illustrates the new idea. Internal stresses are introduced through the geometric constraint of an architected elastomer element to firstly realize hyperdamping inclusions. Namely, a soft, cylindrical and sculpted elastomer element is inserted into a metal shell that has an inner diameter D_i smaller than the element's outer diameter D_o, Fig. 1(a). This is intended to load the elastomer topology at the elastic stability limit. Fig. 1(b) shows finite element modeling results, detailed in Section 2, to illustrate the stable, post-buckled topologies of the elastomer element if the constraint induces a stress beyond criticality. Depending on the design of internal elastomer elements, such as with or without a solid metal cylinder, buckling may or may not occur for given sizes of the metal shell, Fig. 1(c). As will be shown in this report, such factors establish a versatile means for hyperdamping inclusion design and tuning.

Developed in this way and considering the shell to be fixed, the hyperdamping inclusion is an extremely damped spring–mass having a vanishingly small natural frequency, where mass contributions are from the internal elastomer and other internal constituents such as the metal cylinder shown in Fig. 1(c) and the springs refer to the critically-loaded, radially-arrayed beams of the inclusion. The inherent damping constant of this equivalent oscillator is that associated with the elastomer, but the hypothesis of this research is that the relative impact of the finite damping grows enormously upon loading the inclusion at the elastic stability limit. To leverage the inclusion for wave energy capture, we embed them into poroelastic foam where the total inclusion mass (i.e. the shell and what is within) generates an *additional* mass–spring–damper degree-of-freedom

(DOF) due to the host media, Fig. 1(d). The two resulting natural frequencies of this equivalent two DOF system occur at a vanishingly-small value due to the critically buckled constituent and at a (typically low) frequency associated with the total inclusion mass and host media properties [30]. Thus, from an observer's perspective, the lightweight inclusion responds dynamically like an extremely damped single DOF which yields massive vibroacoustic energy damping in a broad frequency bandwidth around and above the low natural frequency associated with the total inclusion resonance. Thus, by leveraging a critically-loaded "hidden" DOF [23,31], in this report we show that the hyperdamping metamaterial exhibits unusual levels of vibration and wave energy attenuation and absorption using a lightweight design that interfaces with the acoustic free field and does not rely on purely resonant phenomena to provide its effects.

The following section describes the fabrication strategies employed to realize the inclusions and presents results from finite element model investigations that guide selection of hyperdamping inclusion design parameters for the targeted softening and buckling behaviors. Then, experimental results are presented which verify the modeling predictions and exemplify the enhanced broadband vibroacoustic energy trapping and attenuation achieved by the new framework of hyperdamping metamaterials. Concluding discussions summarize the findings and future outlooks.

2. Fabrication, modeling, and design of hyperdamping inclusions

The fabrication of the hyperdamping metamaterials is undertaken in several steps. A 3D printer (FlashForge Creator Pro) generates ABS molds which are the negative of the elastomer elements. Silicone (Smooth-On, Inc., Mold Star 15S) is poured into the molds that are previously sprayed with a release agent (Smooth-On, Inc., Ease Release 200), and the samples are removed after the recommended curing time has elapsed. The elastomer samples are cut to 19 mm length and allowed to set at room temperature for a sufficient time prior to further use. If the elastomer samples include interior metal cylinders (6.35 mm outer diameter and 19 mm length) such as the samples shown at right in Fig. 1(c), the cylinders are held in place in the mold so that the silicone cures around the cylinder. Several samples of a given outer elastomer diameter D_o are produced (ranging from $D_o \in [16.38, 18.16]$ mm) whether with solid elastic interior masses or with interior metal cylinders. The elastomer elements produced by this method exhibited a mean standard deviation of outer diameter of 69 μm, which is on the order of the reported resolution of the 3D printer. The mean mass of the inclusions with elastomer and metallic internal masses are 3.42 g and 8.04 g, respectively. Aluminum shells of inner diameter $D_i = 16.56$ mm and thickness 1.25 mm are cut to 19 mm lengths and the elastomer elements are carefully inserted into the shells. This study reports the outcomes of inclusions made with seven rotationally-symmetric voids, as shown in Fig. 1(a), although the following results are generalized to inclusions with at least two voids to realize an annular region around the interior mass such that the mass is capable of buckling under the displacement constraint imposed by the metal shell.

To develop insight on inclusion topological designs that maximize the effective damping properties of the components once embedded into the poroelastic media, a finite element (FE) model is composed using the commercial software package COMSOL Multiphysics (see Supplementary Material in Appendix A for modeling details). The elastomer element designs of interest are those which are loaded around at the elastic stability limit once constrained within the metal shells, such that the softening influences are most prominent. In other words, the goal is to
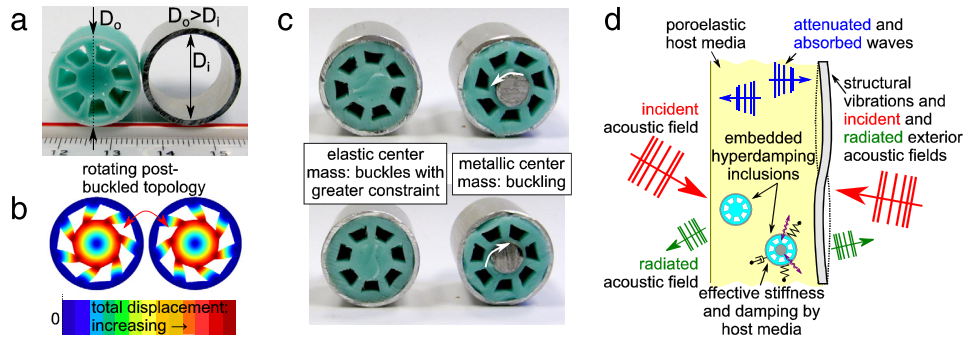
Fig. 1. (a) Inclusion design principle that the elastomer element outer diameter is greater than the inner diameter of the rigid, metal shell. (b) Finite element model results that predict rotational motions for pre- and post-buckled designs. (c) Elastic or metallic center masses buckle for increasing degree of pre-compression upon inserting the elastomer/mass into the metal shell. (d) Illustration of hyperdamping metamaterial with embedded inclusions in poroelastic media to attenuate and absorb incident acoustic waves and structural vibrations.
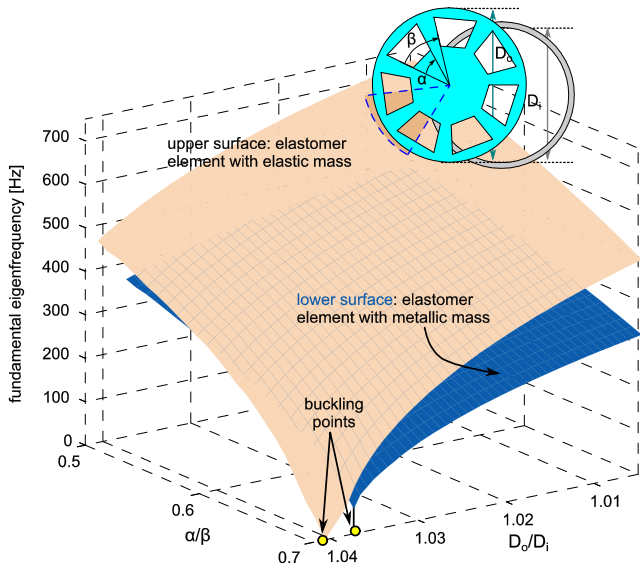

Fig. 2. Top right illustration shows the design parameters of the diametric ratio D_o/D_i and the rotational angle ratio α/β. The surfaces show the influence on the fundamental eigenfrequency of the elastomer element by tailoring these parameters. The upper surface considers the elastomer element with the same internal elastomer mass while the lower surface considers the metallic mass in the elastomer element.

design the elastomer elements to be extremely close to the point of buckling to maximize the effective damping properties when the inclusion (shell and elastomer element) is embedded into the poroelastic foam. As previously shown, the resonance of the embedded inclusion in the foam is influenced by factors that consider such inclusions as equivalent lumped masses within a distributed elastic media [26]. The rotational symmetry of the molded elastomer designs considered here is inspired from the recent finding that applied stress on an instability-driven periodic metamaterial induces a symmetry breaking at the critical buckling stress [16], Fig. 1(b). Although several design parameters may be tailored to sculpt the topology in ways that provide means to critically stress the elastomer elements, here the focus is on changing the diametric ratio D_o/D_i and the ratio of rotation angles α/β in an elastomer element having seven voids, top of Fig. 2. The rotational angle ratios α/β considered are set by the limits of fabrication using the current practice, while the diametric ratios D_o/D_i must be >1 to induce buckling.

As observed in the FE model results in Fig. 2, the decrease of the absolute value of the lowest eigenfrequency, which vanishes at the buckling point, may span orders of magnitude via tailoring the diametric and rotational angle ratios. The figure presents

results for cases in which the interior mass of the elastomer element is also elastomer material (upper surface) or the elastomer element contains the metallic interior mass (lower surface) which are the compositions exhibited in Fig. 1(c). It is observed that for a given selection of rotational angle and diametric ratios, the inclusion with elastomer inner mass possesses the higher fundamental eigenfrequency. By strategically tailoring these ratios, the eigenfrequency can be adjusted from values in the 100s of Hz to the buckling point (0 Hz), which stresses the elastomer element at the elastic stability limit. The shape of this fundamental mode, as well as the first buckling mode, is exemplified in the FE model results in Fig. 1(b). From the model predictions presented in Fig. 2, rotational angle ratios at the limits of the current fabrication capabilities ($\alpha/\beta \approx 0.7$) are required to buckle the elastomer elements within a reasonable amount of geometric constraint $D_o/D_i < 1.05$. As observed empirically, values of such constraint above this amount may warp the elastomer topology at the contact surface with the metal shell, thus violating the FE model assumptions and inhibiting uniform compressive stress at the contact. The results in Fig. 2 also indicate that the samples with metallic inner masses buckle for smaller values of both ratios (lower surface) than those required for the samples having the elastomer masses (upper surface). Considering the rotationally-symmetric unit of the inclusion highlighted by the dashed section in the top right inset of Fig. 2, each radially-arrayed beam is axially constrained between the outer metal shell and the inner mass. It is known that the presence of compliance in the boundary conditions of axially-loaded beams increases the loads required to buckle the beam [32], which verifies the finding here that the comparatively rigid metallic inner masses require small diametric ratios to load the inclusions at the elastic stability limit for hyperdamping effects.

3. Fabrication and experimentation of hyperdamping metamaterials

Using the insights derived from the FE model analysis, hyperdamping metamaterials are produced by embedding the strategically designed inclusions into 50.4 mm thick open cell polyurethane foam (Foam Factory, Inc.). In anticipation of the investigations of absorption coefficient as measured in the impedance tube, cylindrical foam samples are cut to a diameter of approximately 82 mm. The foam is then cut into two equal thicknesses, and a centrally-located crevice is extracted into which the hyperdamping inclusion is placed and secured via spray glue (HDX Spray Adhesive), Fig. 3(a). Portions of the foam extracted in the prior operation are returned to their positions and the entire specimen is glued back into one piece. In all procedures, the glue is lightly sprayed so as to not adversely impact the vibroacoustic
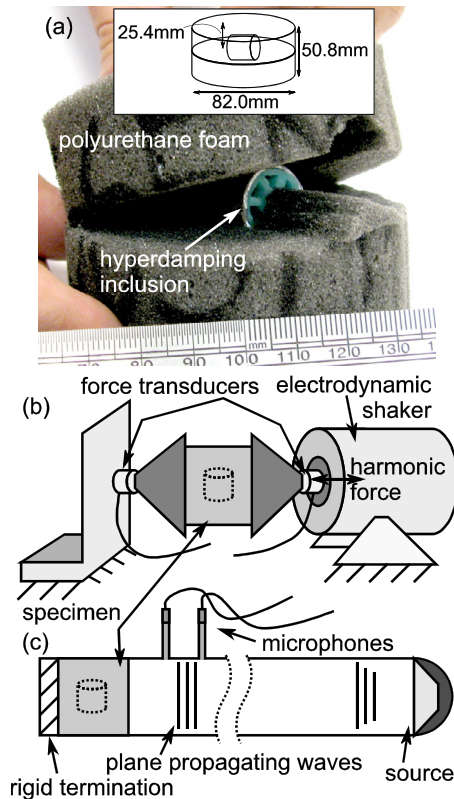
Fig. 3. (a) Hyperdamping metamaterial specimen prior to assembly. (b) Force transmissibility and (c) absorption coefficient experiment schematics.

properties of the polyurethane foam. By this fabrication, the resulting hyperdamping metamaterial specimen appears externally identical from the original cylinder of foam from which it was derived, apart from a small seam of spray glue visible around the perimeter. In addition, by extracting the inner material, the foam is not under additional stresses once re-assembled via the glue. Using the current design parameters, all hyperdamping inclusions constituted a 2% volume fill ratio respecting the whole metamaterial volume, and result in an effective metamaterial specimen density of 48 kg · m^{-3} (compared to the polyurethane foam density 34 kg · m^{-3}). This is significantly less than the effective density of recent metamaterials leveraging resonance- and bandgap-based phenomena (around 1500 kg·m^{-3} [16] or >2000 kg·m^{-3} [11]) and is more comparable to the density of various acoustical materials used in automotive and aerospace applications [7].

By a linear elastic FE model (see Supplementary Material in Appendix A), the primary vibration modes of the inclusion in the foam are seen to occur around the frequency band 175–275 Hz; for the metallic inner mass, these relevant resonances are at the lower end of this band, while for the elastomer mass they are at the higher end. As a result, it is anticipated that the greatest evidence of broadband energy absorption provided by the hyperdamping metamaterials will be found within this bandwidth. Above this frequency band, the modal density increases significantly per octave and the higher frequency modes are mostly associated with large deformations of the foam itself. Traditionally, periodic metamaterials are designed to leverage the lower frequency resonant modes for drastic vibroacoustic attenuation at the specific eigenfrequencies [33]. In contrast, here it will be shown that the hyperdamping metamaterial, using only a single inclusion, facilitates strongly damped resonant properties in this frequency band as well as at higher frequencies where the modal density grows; the result is a notably broadband, and hence robust, energy trapping and attenuation effect.

To characterize the impact of the hyperdamping inclusions, experiments are first conducted with the foam on its own, having been previously cut in half and re-assembled by spray glue, and also using a conventional resonance-based metamaterial design that includes the foam and a single inclusion consisting of lumped elastomer cured in the metal shell. The conventional approach is also similar to the strategy employed by the previous studies on poroelastic metamaterials where lumped mass (often metal) inclusions have been considered [26,27]. All experiments are carried out in an environmentally-controlled room at 22.8 °C and 37% humidity. The force transmissibility through and acoustic absorption coefficient of the specimens are evaluated as schematically shown in Fig. 3((b), (c)) (see Supplementary Material in Appendix A). The resulting force transmissibility data represent the averaged result from 80 independent measurements when the electrodynamic shaker (LabWorks, ET-140) is driven with white noise filtered from 30 to 1500 Hz and data is acquired using input and output force transducers (PCB Piezotronics, 208C01). The acoustic absorption data are derived from pressure measurements taken in the impedance tube with the acoustic source providing white noise from 50 to 1600 Hz; we average the results from 80 independent measurements obtained from the two microphones (PCB Piezotronics, 130E20), in accordance with ASTM E1050-12, to derive the absorption coefficient [34].

Fig. 4 presents the results of force transmissibility amplitude (left column) and acoustic absorption coefficient (right column) for the poroelastic foam itself (dotted curves), the resonant metamaterial (dashed curves, and see (c) top right illustration), and the hyperdamping metamaterial (solid curves, and see (c) top left illustration) using a diametric ratio of $D_o/D_i = 1.051$, elastomer inner mass, and rotational angle ratio $\alpha/\beta = 0.70$. According to the FE model results shown in Fig. 3, this diametric ratio is in excess of the ideal design at the elastic stability limit, and thus the hyperdamping specimen used in the comparison of Fig. 4 is not optimized. As described above, the modes associated with the total mass of the inclusion displacing greatly with respect to the foam occur in the frequency band 175–275 Hz, while modes below and above this range the modes are mostly associated with large deformations of the foam itself. Thus, in Fig. 4(a), the measurements of force transmissibility (FT) reveal great similarity in response trends at frequencies outside of this range while in the range there are notable differences to consider. For instance, the narrowband FT shows that the resonant and non-optimized hyperdamping metamaterials provide approximately similar reductions across the 175–275 Hz band, compared to the FT of the foam itself, wherein occur their principal resonances as embedded in the foam elastic matrix. Yet, considering the 1/3-octave band results, Fig. 4(b), it is found that from 200 to 630 Hz, the hyperdamping metamaterial provides an average of 1.2 dB greater FT reduction than the resonant metamaterial. In addition, the absorption coefficients in the narrowband and 1/3-octave band comparisons of Fig. 4(c) and (d), respectively, reveal similar enhancement of the acoustic wave attenuation by virtue of the inclusions. These results show that a non-optimized hyperdamping metamaterial can provide comparable or greater absorption of vibroacoustic energy than a counterpart, resonant metamaterial all the while the hyperdamping inclusion design constitutes only 48% of the mass of the resonant inclusion.

Having assessed the merits of the hyperdamping concept with respect to the conventional resonant metamaterial approach, we next evaluate the impact of more effective hyperdamping inclusion design as informed from the FE model results of Fig. 2. In this way, we test the foundational hypothesis of this research that inclusion designs nearest to the elastic stability limit cultivate the greatest damping effects. By the reductions in the FT amplitude with respect to the specimen consisting of only poroelastic foam,
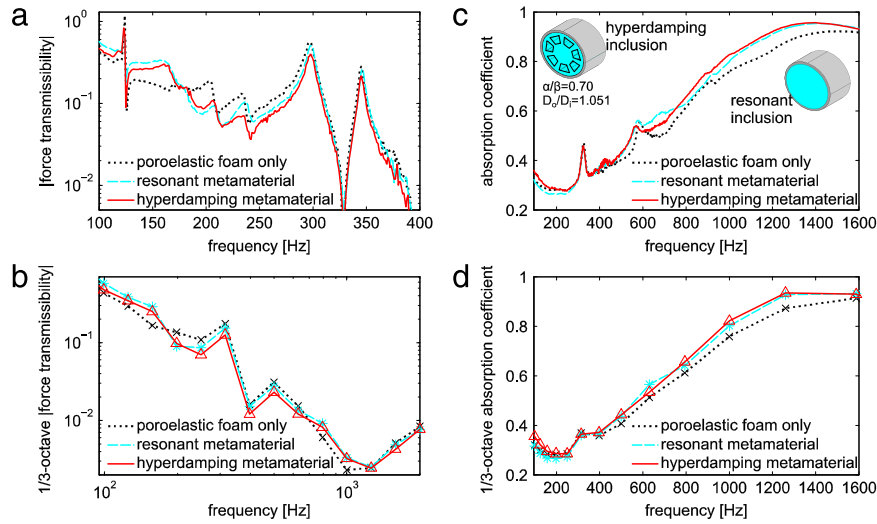
Fig. 4. Measurements of narrowband and 1/3-octave band results of (a,b) force transmissibility amplitude (FT) and (c,d) acoustic absorption coefficient. Comparison is made among the (dotted curves) poroelastic foam itself, (dashed curves) the resonant metamaterial with lumped elastomer and shell inclusion (see (c) top right illustration), and (solid curves).
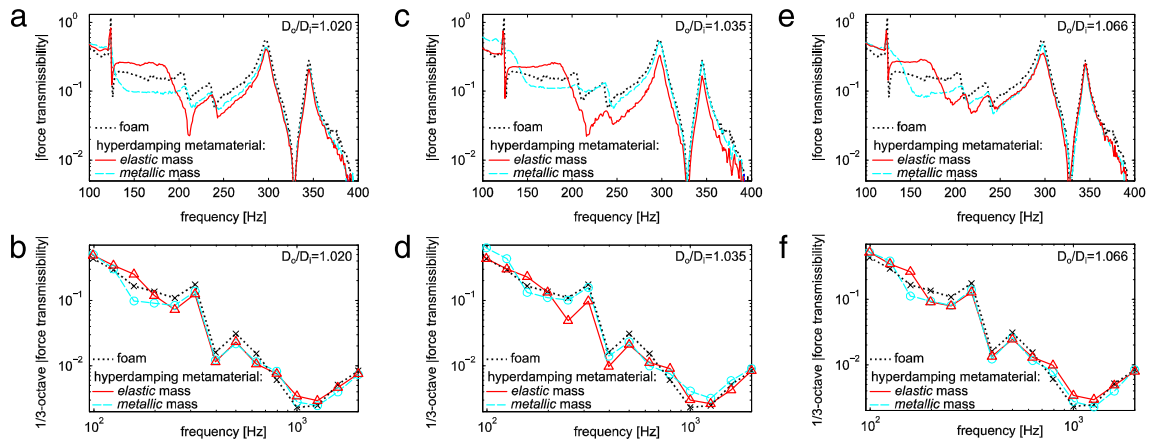

Fig. 5. Measurements of force transmissibility amplitude (FT). Dotted curves denote results for the control specimen; solid curves denote results for the hyperdamping metamaterial with elastomer inner mass; dashed curves denote results for the hyperdamping metamaterial with metallic inner mass. Narrowband and 1/3-octave band results for the hyperdamping specimen designs having diametric ratio (a,b) $D_o/D_i = 1.020$, (c,d) $D_o/D_i = 1.035$, and (e,f) $D_o/D_i = 1.066$.

the measurements in the top row in Fig. 5 show that the broadband energy absorption and attenuation is prominent across the range of about 175–225 Hz for the hyperdamping specimens having the metallic inner mass, Fig. 5(a), while for the specimens with elastic inner mass the energy capture is more apparent around 200–275 Hz, Fig. 5(c). The FE model results in Fig. 2 indicate that the critical design point occurs for smaller values of the diametric ratio D_o/D_i using the metallic inner masses, when the rotational angle ratio α/β is held constant. The FT measurements in both the narrowband and 1/3-octave evaluations of Fig. 5 verify this design methodology and justify the research hypothesis. Namely, the hyperdamping metamaterial with metallic inner mass generates the greatest broadband energy dissipation for the smaller ratio $D_o/D_i = 1.020$ (29.1% mean reduction of FT in 1/3-octaves from 157 to 630 Hz with respect to the control specimen) while the specimen with elastomer inner mass yields maximum broadband performance for the greater ratio $D_o/D_i = 1.035$ (41.2% mean enhancement of FT reduction in 1/3-octaves from 250 to 630 Hz with respect to the control specimen). The reductions to FT well above the primary resonances of the inclusions in the poroelastic material are due to the increasing modal density which occurs above about 275 Hz thus introducing means to magnify the energy dissipation properties in the mid frequency

range. These are significant increases in the *broadband* absorbed and attenuated vibration energy, particularly considering that the hyperdamping inclusions account for only 2% of the total specimen volume. Importantly, these enhancements to the energy dissipation are reduced if the diametric ratio is changed to be deliberately away from the elastic stability limit. For example, the specimens having the metallic inner masses are less effective in the broadband reduction of FT when $D_o/D_i > 1.020$, Fig. 5((c), (e)), which corresponds to post-buckled configurations of the elastomer element as observed empirically; specimens with elastomer inner masses have reduced energy attenuation performance for $D_o/D_i > 1.035$, Fig. 5(e), which likewise corresponds to post-buckling of the elastomer element. These results validate the hypothesis of this research that the hyperdamping effects are due to the extreme softening of the inclusions and not simply to compressing the inclusions beyond the buckling point.

The top row of Fig. 6 presents the narrowband measurements of absorption coefficient while the bottom row provides the corresponding 1/3-octave band results. Of note, the polyurethane foam is itself very acoustically absorptive such that enhancement of this property using a single, embedded hyperdamping inclusion appears to be a challenging goal at the outset. Yet, as seen in the top row of Fig. 6, due to the presence of the hyperdamping
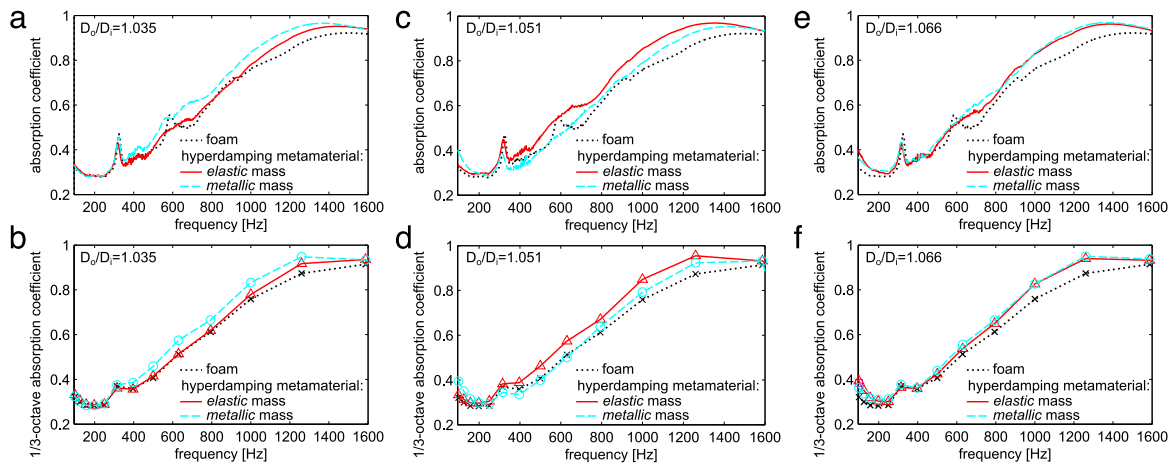
Fig. 6. Measurements of absorption coefficient. Dotted curves denote results for the control specimen; solid curves denote results for the hyperdamping metamaterial with elastomer inner mass; dashed curves denote results for the hyperdamping metamaterial with metallic inner mass. Narrowband and 1/3-octave band results for the hyperdamping specimen designs having diametric ratio (a,b) $D_o/D_i = 1.035$, (c,d) $D_o/D_i = 1.051$, and (e,f) $D_o/D_i = 1.066$.

inclusions the absorption coefficient of the baseline poroelastic foam is increased from frequencies of about 400 to 1400 Hz, across which the modal density is sufficiently great. This improvement is greatest for the inclusions having metallic masses when employing the smaller value of the diametric ratio, Fig. 6(a), $D_o/D_i = 1.035$, which agrees with the FE model predictions. Using this inclusion composition, across the 500–1260 Hz 1/3-octave bands the mean absolute enhancement of the absorption coefficient from control specimen levels is 0.063, Fig. 6(b). Also in agreement with the design cues derived from the FE investigations, the hyperdamping inclusions with elastomer inner masses are more effective at increasing the energy dissipation (and hence absorption coefficient) for a greater value of diametric ratio, Fig. 6(c), yielding a mean absolute absorption coefficient improvement from the control specimen results of 0.045 across the 500–1260 Hz 1/3-octave bands, Fig. 6(d). Indeed, for both of the prior design cases that strategically leverage the hyperdamping effect, the increase in the absorption coefficient over the control specimen is uniform across this broad frequency band. Finally, when the inclusions are constrained by diametric ratios greater than the prior values, Fig. 6((e), (f)) show that the performances of the specimens are reduced from the peak achievements realized when the elastomer elements are compressed around the elastic stability limit. Thus, again verifying the hypothesis of this research, the exceptional softening of the inclusion design is the origin of the hyperdamping effects, which invests the metamaterial with remarkable, broadband vibroacoustic energy dissipation properties using a negligible change (2%) to the host media volume due to the embedded inclusion.

4. Discussion and conclusions

As employed here, "hyperdamping" indicates a unnaturally large ratio of damping to inertial forces in consequence to design- or constraint-based factors imposed upon an intelligently architected inclusion topology. In the present implementation, the selection of diametric ratio for a given elastomer element topology enables the extreme softening which is characteristic of loading conditions at the elastic stability limit. Other researchers have realized similar anomalous dissipative phenomena via applied compressive stress [35], ferroelectric domain switching [36], and temperature control [22]. Contrasting these approaches, the strategy employed here to realize hyperdamping within the poroelastic media is passive, non-destructive to the host material, and not subject to major deviation over time by

hysteretic influences, thus making the proposed hyperdamping metamaterials more viable for practical applications. Moreover, this study focuses on the impact of an *individual* inclusion upon the resulting vibroacoustic properties of the metamaterial. This contrasts with previous studies that have exemplified the roles of periodicity towards magnifying the energy absorption possible in resonant metamaterials or phononic crystals [10,13,27,29,33,37]. Yet, based on the experimental evidence uncovered in Figs. 4, 5, and 6, which supports the modeling insights in Fig. 2, substantial broadband energy trapping and attenuation is achievable even when employing just one hyperdamping inclusion at a 2% volume fill in the poroelastic media.

Building upon recent advancements in the intelligent use of elastic instabilities and lumped-mass inclusions in elastic and poroelastic material systems, this research introduced a new framework of hyperdamping metamaterials to realize significant broadband energy trapping and attenuation while retaining the advantages of a lightweight solution viable for diverse noise and vibration control applications. Because the hyperdamping effects are not reliant upon the resonance- or bandgap-based phenomena of conventional metamaterials and phononic crystals, the effectiveness of the energy attenuation is more robust for working conditions where the peak frequencies of vibroacoustic energy may vary in time. In this way, the lightweight, hyperdamping metamaterials have practical benefits over contemporary counterparts.

Appendix A. Supplementary data

Supplementary material related to this article can be found online at http://dx.doi.org/10.1016/j.eml.2016.05.017.

References

[1] L. Cremer, M. Heckl, B.A.T. Petersson, Structure-Borne Sound: Structural Vibrations and Sound Radiation at Audio Frequencies, Springer, Berlin, 2005.
[2] S. Krödel, T. Delpero, A. Bergamini, P. Ermanni, D.M. Kochmann, 3D auxetic microlattices with independently controllable acoustic band gaps and quasi-static elastic moduli, Adv. Energy Mater. 16 (2014) 357–363.

[3] G. Ma, M. Yang, S. Xiao, Z. Yang, P. Sheng, Acoustic metasurface with hybrid resonances, Nature Mater. 13 (2014) 873–878.

[4] D.A. Bies, C.H. Hansen, Engineering Noise Control: Theory and Practice, Spon Press, London, 2006.

[5] E.E. Ungar, The status of engineering knowledge concerning the damping of built-up structures, J. Sound Vib. 26 (1973) 141–154.

[6] J. Blauert, N. Xiang, Acoustics for Engineers, Springer, Berlin, 2009.

[7] J.F. Allard, N. Atalla, Propagation of Sound in Porous Media: Modelling Sound Absorbing Materials, John Wiley & Sons, Ltd., Chichester, 2009.

[8] K. Idrisi, M.E. Johnson, A. Toso, J.P. Carneal, Increase in transmission loss of a double panel system by addition of mass inclusions to a poro-elastic layer: a comparison between theory and experiment, J. Sound Vib. 323 (2009) 51–66.

[9] T. Sain, J. Meaud, G. Hulbert, E.M. Arruda, A.M. Waas, Simultaneously high stiffness and damping in a class of wavy composites, Compos. Struct. 101 (2013) 104–110.

[10] M.I. Hussein, M.J. Frazier, Metadamping: an emergent phenomenon in dissipative metamaterials, J. Sound Vib. 332 (2013) 4767–4774.

[11] E. Baravelli, M. Ruzzene, Internally resonating lattices for bandgap generation and low-frequency vibration control, J. Sound Vib. 332 (2013) 6562–6579.

[12] G. Acar, C. Yilmaz, Experimental and numerical evidence for the existence of wide and deep phononic gaps induced by inertial amplification in two-dimensional solid structures, J. Sound Vib. 332 (2013) 6389–6404.

[13] M.I. Hussein, M.J. Leamy, M. Ruzzene, Dynamics of phononic materials and structures: historical origins, recent progress, and future outlook, Appl. Mech. Rev. 66 (2014) 040802.

[14] M. Nouh, O. Aldraihem, A. Baz, Wave propagation in metamaterial plates with periodic local resonances, J. Sound Vib. 341 (2015) 53–73.

[15] B. Florijn, C. Coulais, M. van Hecke, Programmable mechanical metamaterials, Phys. Rev. Lett. 113 (2014) 175503.

[16] P. Wang, F. Casadei, S. Shan, J.C. Weaver, K. Bertoldi, Harnessing buckling to design tunable locally resonant acoustic metamaterials, Phys. Rev. Lett. 113 (2014) 014301.

[17] S. Shan, S.H. Kang, J.R. Raney, P. Wang, L. Fang, F. Candido, J.A. Lewis, K. Bertoldi, Multistable architected materials for trapping elastic strain energy, Adv. Mater. 27 (2015) 4296–4301.

[18] D. Restrepo, N.D. Mankame, P.D. Zavattieri, Phase transforming cellular materials, Extreme Mech. Lett. 4 (2015) 52–60.

[19] S. Shan, S.H. Kang, P. Wang, C. Qu, S. Shian, E.R. Chen, K. Bertoldi, Harnessing multiple folding mechanisms in soft periodic structures for tunable control of elastic waves, Adv. Funct. Mater. 24 (2014) 4935–4942.

[20] N. Hu, R. Burgueño, Buckling-induced smart applications: recent advances and trends, Smart Mater. Struct. 24 (2015) 063001.

[21] Z.P. Bažant, L. Cedolin, Stability of Structures: Elastic, Inelastic, Fracture, and Damage Theories, World Scientific Publishing Co., Hackensack, New Jersey, 2010.

[22] Y.C. Wang, M. Ludwigson, R.S. Lakes, Deformation of extreme viscoelastic metals and composites, Mater. Sci. Eng. A 370 (2004) 41–49.

[23] I. Antoniadis, D. Chronopoulos, V. Spitas, D. Koulocheris, Hyper-damping peroperties of a stiff and stable linear oscillator with a negative stiffness element, J. Sound Vib. 346 (2015) 37–52.

[24] L.N. Virgin, R. Wiebe, On damping in the vicinity of critical points, Phil. Trans. R. Soc. A 371 (2013) 20120426.

[25] D.J. Inman, Engineering Vibration, Prentice Hall, Saddle River, New Jersey, 2001.

[26] K. Idrisi, M.E. Johnson, D. Theurich, J.P. Carneal, A study on the characteristic behavior of mass inclusions added to a poro-elastic layer, J. Sound Vib. 329 (2010) 4136–4148.

[27] A.C. Slagle, C.R. Fuller, Low frequency noise reduction using poro-elastic acoustic metamaterials, in: Proceedings of the 21st AIAA/CEAS Aeroacoustics Conference, Dallas, Texas, USA, 2015, AIAA 2015-3113.

[28] C. Lagarrigue, J.P. Groby, V. Tournat, O. Dazel, O. Umnova, Absorption of sound by porous layers with embedded periodic arrays of resonant inclusions, J. Acoust. Soc. Am. 134 (2013) 4670–4680.

[29] J.P. Groby, C. Lagarrigue, B. Brouard, O. Dazel, V. Tournat, Using simple shape three-dimensional rigid inclusions to enhance porous layer absorption, J. Acoust. Soc. Am. 136 (2014) 1139–1148.

[30] Z. Wu, R.L. Harne, K.W. Wang, Energy harvester synthesis via coupled linear-bistable system with multistable dynamics, J. Appl. Mech. 81 (2014) 061005.

[31] N. Kidambi, R.L. Harne, K.W. Wang, Adaptation of energy dissipation in a mechanical metastable module excited near resonance, J. Vib. Acoust. 138 (2016) 011001.

[32] J. Mayers, B.G. Wrenn, Combined influence of higher-order linear effects and nonlinear effects on the lateral vibration behavior of solid and sandwich beams, SUDAER 208, 1964.

[33] X.N. Liu, G.K. Hu, G.L. Huang, C.T. Sun, An elastic metamaterial with simultaneously negative mass density and bulk modulus, Appl. Phys. Lett. 98 (2011) 251907.

[34] ASTM International, "Standard Test Method for Impedance and Absorption of Acoustical Materials Using a Tube, Two Microphones and a Digital Frequency Analysis System," ASTM E1050-12, 2012.

[35] L. Dong, R.S. Lakes, Advanced damper with negative structural stiffness elements, Smart Mater. Struct. 21 (2012) 075026.

[36] C.S. Wojnar, J.B. le Graverend, D.M. Kochmann, Broadband control of the viscoelasticity of ferroelectrics via domain switching, Appl. Phys. Lett. 105 (2014) 162912.

[37] S. Krödel, N. Thomé, C. Daraio, Wide band-gap seismic metastructures, Extrem. Mech. Lett. 4 (2015) 111–117.

Trapping and attenuating broadband vibroacoustic energy with hyperdamping metamaterials

Ryan L. Harne*, Yu Song, Quanqi Dai

Department of Mechanical and Aerospace Engineering, The Ohio State University, Columbus, OH 43210, USA

* Corresponding author, email: harne.3@osu.edu

Supplementary Material

1. Eigenfrequency analysis and design of the hyperdamping inclusions

The finite element (FE) model to study the effective topological composition of the hyperdamping inclusions utilizes the geometry exemplified in the main text Figure 2 at the top inset, assuming plane strain conditions apply for a first approximation of the principal eigenfrequencies and modes. Material properties are therefore required for inner metal cylinders (if applicable) and for the elastomer elements. The steel metal cylinders are modeled as a linear elastic material having density, Young's modulus, and Poisson's ratio, respectively, $\rho = 7800$ kg.m^{-3}, $E = 200 \times 10^9$ Pa, and $\nu = 0.30$. Previous studies have indicated that similar variants of the silicone used here to create the elastomer elements are adequately characterized using Neo-Hookean, hyperelastic material models [1] [2]. In such cases, the strain energy density is expressed using

$$W = \frac{1}{2}\mu_0\left(\bar{I}_1 - 3\right) + \frac{1}{2}K_0\left(J - 1\right)^2$$

where μ_0 and K_0 are the initial shear and bulk moduli, $J = \det \mathbf{F}$ is the determinant of the deformation gradient $\mathbf{F} = \partial\mathbf{x}/\partial\mathbf{X}$ found respecting the current $\mathbf{x}$ and reference $\mathbf{X}$ configurations, and $\bar{I}_1 = tr\left(\bar{\mathbf{F}}^T\bar{\mathbf{F}}\right)$ is computed from the distortional tensor $\bar{\mathbf{F}} = \left(J^{1/3}\mathbf{I}\right)^{-1}\mathbf{F}$ where $\mathbf{I}$ is the identity matrix [1]. For the silicone material employed in this research, representative parameters of $\mu_0 = 250$ kPa and $K_0 = 6.25$ MPa are employed in the FE computations while the density is $\rho = 1145$ kg.m^{-3} as measured. The boundary conditions constrain the normal displacement of the elastomer element outer diameter in accordance with the constraint imposed by the ratio D_o/D_i. An eigenfrequency analysis is carried out to evaluate the influence upon the lower-order eigenfrequencies due to the variation in the ratios α/β, which characterizes the unconstrained topology of the elastomer element, and D_o/D_i, which quantifies the nearness to the critical buckling stress upon the elastomer element topology. Additional design variables are being considered in ongoing studies for their roles on the frequency sensitivities of the hyperdamping inclusions. However, a key design theme is that the sculpted beams that support an internal mass must be arrayed radially from the inclusion center, otherwise the compression provided by the geometric shell

constraint would be prevented from causing a buckling of the topology. To illustrate the change in the lower order eigenfrequencies in consequence to the constraint imposed by the metal shell, Figure S1 shows results from this FE model for the case in which the rotational angle ratio α/β=0.70 while the diametric ratio D_o/D_i is varied. From the FE model results at right, it is evident that the second, third, and fourth eigenfrequencies do not significantly change due to the critical stressing that occurs when the elastomer element topology is designed to lead to buckling effects. This may be explained by the fact that these mode shapes are not rotationally symmetric, as shown in the right part of Figure S1, while the critical constraint that leads to buckling is one which uniformly applies to the elastomer element around the full perimeter.
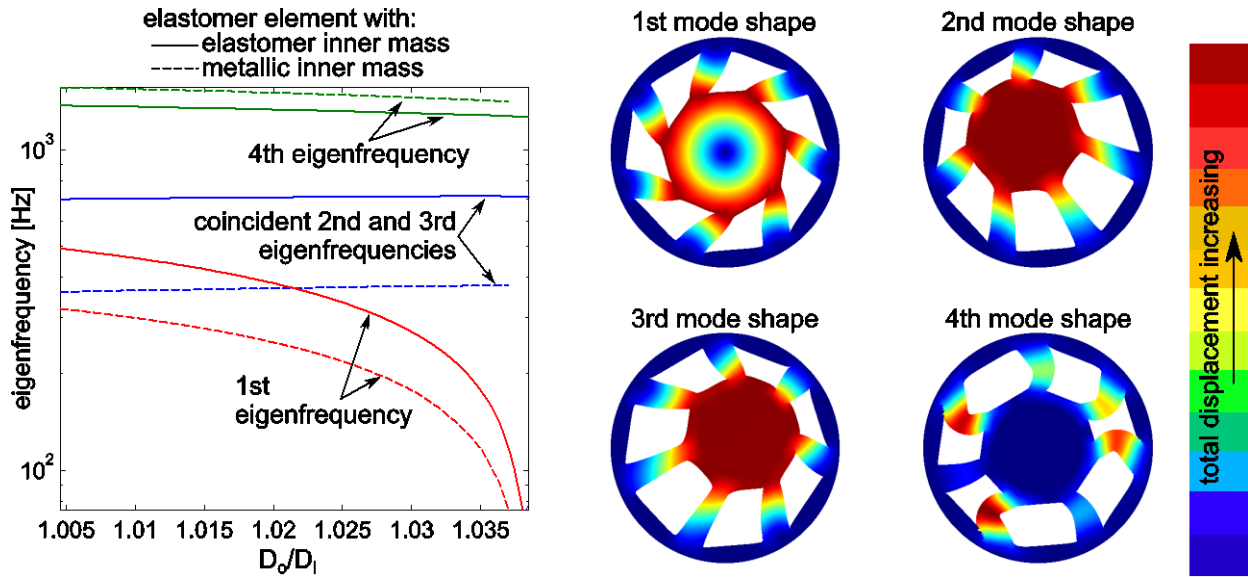

Figure S1. Comparison of eigenfrequency variation among the four lowest eigenfrequencies (at left) and the corresponding mode shapes (at right). The dotted curves at right indicate that the inner mass of the inclusion is metallic while the solid curves indicate results when the inner mass is composed of the elastomer material.

2. Eigenfrequency analysis of the hyperdamping metamaterials

A FE model is created to assess the distribution of the structural eigenfrequencies and modes for the hyperdamping inclusion once embedded into the polyurethane foam. By such an evaluation, one is able to more effectively assess the impact of the inclusions since the greatest magnification of the damping effects are around the frequencies associated with these resonances, assuming they are significantly excited by the source input [3]. As observed macroscopically, the result will be that these resonances, often associated with resonance-based metamaterials [4], will appear to be strongly damped.

The FE model geometry is identical to the experimental geometry as detailed in the main text, top of Figure 3. In this model, the polyurethane foam is considered to be a linear elastic material. Thus, poroelastic coupling is neglected, which is justified by the focus on small-amplitude, relatively low frequency force transmissibility and acoustic-elastic wave propagation, where the linear elastic characteristics of the polyurethane foam are more apparent [5]. The polyurethane material properties are given to be ρ =30 kg.m⁻

[3], $E = 7 \times 10^4$ Pa, and $\nu = 0.41$. The inclusion is modeled as an effective lumped mass of uniform density, Poisson's ratio $\nu = 0.33$, and high stiffness $E = 200 \times 10^9$ Pa in accordance with the assumption that it is only a cylindrical mass embedded into the foam. The uniform density of this mass is therefore the average mass of the inclusions for a given D_o (whether with inner elastomer or metallic cylindrical mass) divided by the inclusion volume. Consideration of the inclusion as a uniform body is theoretically justified by the fact that the vanishing fundamental eigenfrequency of the hyperdamping inclusion means that the natural frequencies of the composite inclusion components (shell and elastomer element) as embedded into the foam media are primarily due to the total dynamic mass of the composite [3] [6]. This contrasts to considering the inclusion internals as possessing additional degrees of freedom; under the unique condition of the critical buckling constraint which yields the hyperdamping effects, the vanishing principal stiffness contribution indicates that the effective response of the inclusion is significantly first-order and more representative of a damping effect rather than like an additional mass-spring-like degree of freedom.

In this FE model, one circular surface of the metamaterial is fixed while the opposing circular face is free to move in the direction normal to the surface but may not rotate. This set of constraints is identical to that which is employed in the force transmissibility experiments. The results of the FE analyses are shown in Figure S2 in terms of the kinetic energy density associated with each eigenfrequency. Thus, the plot provides information on the spectral distribution of the eigenmodes as well as of the significance of the global system energy associated with the mode. The square data points indicate the FE model results in which the lumped cylindrical inclusions are characterized according to the average density of hyperdamping inclusions with elastomer inner masses (approximately 1238 kg.m^{-3}), while the circles denote the results respecting hyperdamping inclusions with metallic inner masses (approximately 2090 kg.m^{-3}). The modes are found to be the result of three primary phenomena. The lowest frequency mode in each case is associated with uniform (in-phase) compression/elongation of the metamaterial and inclusion. A mid frequency range of modes occurs wherein the inclusions are seen to exhibit large deformations and/or rotations within the foam, while the corresponding eigenfrequencies occur at values corresponding to the total inclusion mass (and are thus distinct comparing the two inclusion types shown in Figure S2). As a result of these large excursions of the inclusions, the greatest broadband damping effect is anticipated to occur in this bandwidth around 175 to 325 Hz. Finally, a higher frequency range of modes occurs characterized by large deformations of the foam while the inclusions are relatively stationary. Since there is comparatively little displacement of the inclusions in contribution to these modes, they occur at almost the same frequencies when considering the two types of inclusions evaluated in Figure S2. These results exemplify the fact that energy trapping occurs primarily at the lower frequencies associated with a select number of resonances possessing high kinetic energy density while at high frequencies the energy loss is due to highly modal density resulting in stochastic-like vibrations that resistively dissipate energy. Thus, this helps to explain why the energy trapping appearing in the force transmissibility experiments (Figure 4 and 5 main text) is mostly localized in the frequency band <600 Hz while the absorption coefficient measurements (Figure 4 and 6 main text), which do not significantly excite lower frequency modes, give greater indications of the

high frequency losses associated with the lower-energy and higher frequency modes that are finely spaced apart in the spectrum.
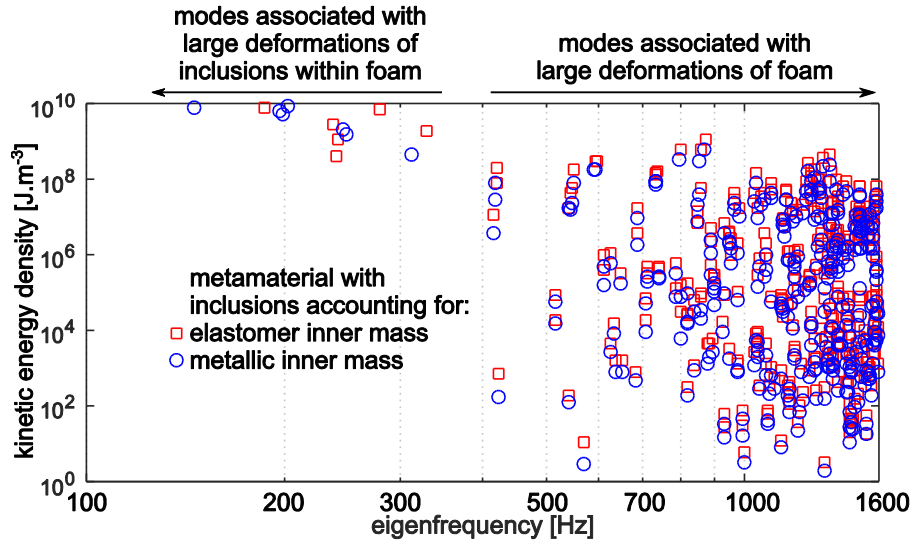

Figure S2. Eigenfrequency distribution and corresponding kinetic energy density of the mode. Squares indicate the results in which the lumped cylindrical inclusions are characterized according to the average density of hyperdamping inclusions with elastomer inner masses, while the circles denote the result respecting hyperdamping inclusions with metallic inner masses.

3. Experimental arrangements, methods, and data post-processing

Force transmissibility experiments are conducted using the arrangement shown in Figure S3. The experiments are carried out on an optical isolation table to prevent potential building motions from interfering with the measurements. White noise filtered from 30 to 1500 Hz is used to drive the electrodynamic shaker which acts on the input force transducer. An output force transducer is attached to a grounded, rigid aluminum frame. As illustrated in the main text Figure 3 and as shown in Figure S3, the force transducers are affixed to force expanders composed from acrylic PMMA which are many orders of magnitude stiffer than the polyurethane foam. The expanders' stiffness inhibits the possibility that the measured forces are different than those transmitted to the hyperdamping metamaterial specimens. The expanders also ensure that the force is equally distributed across the full surfaces of the cylindrical metamaterial specimen so as to evaluate only the one-dimensional force transmissibility property of the specimens through their thickness. Acquired data are sampled at 16384 Hz and are filtered from 20 to 2000 Hz using a fourth-order bandpass infinite impulse response filter prior to further computation. Then, the force transmissibility of the 80 independent measurements is determined and the average of the results is taken. One-third-octave band values are taken in conformance to traditional methods [7].
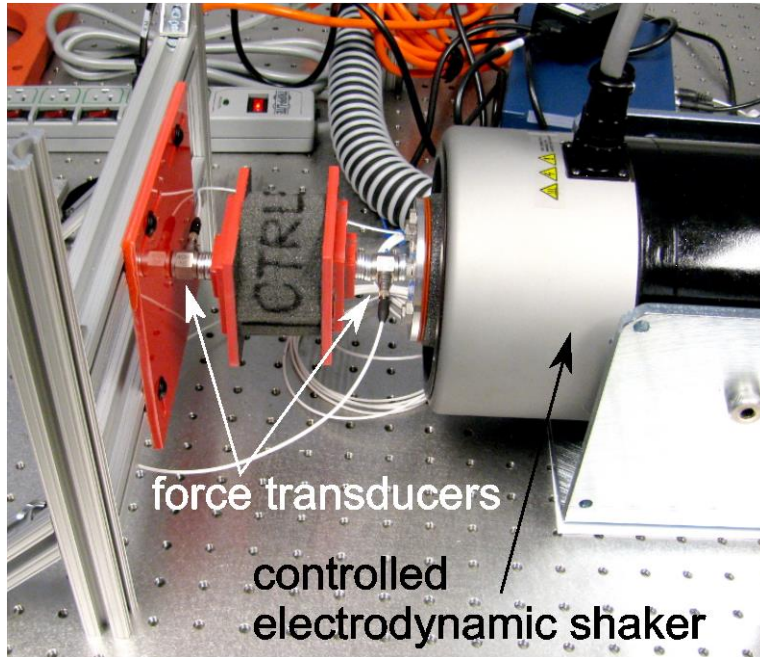
Figure S3. Experimental apparatus employed to measure force transmissibility.

Absorption coefficient measurements are taken using the impedance tube setup as shown in Figure S4. The tube length from acoustic source to specimen surface is approximately 575 mm. The cylindrical metamaterial specimens are mounted in a way such that the surface of the specimen which faces the propagating wave is normal to the direction of wave propagation, ensuring that reflections are likewise normal. Data from the microphones are sampled at 51200 Hz and filtered from 20 to 2000 Hz using a fourth-order bandpass infinite impulse response filter prior to further computation. Then, the acoustic absorption coefficient as determined from the 80 independent measurements is averaged. One-third-octave band values are computed according to traditional methods.
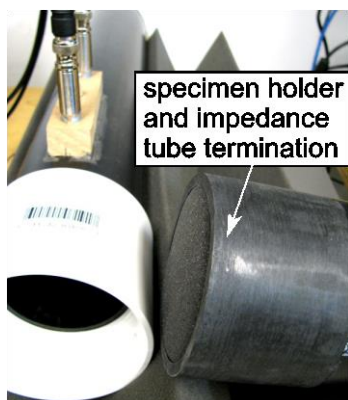

Figure S4. Experimental apparatus employed to measure acoustical absorption coefficient.

References

[1] S. Shan, S.H. Kang, J.R. Raney, P. Wang, L. Fang, F. Candido, J.A. Lewis, and K. Bertoldi, Multistable architected materials for trapping elastic strain energy. Advanced Materials 27 (2015) 4296-4301.

[2] S. Shan, S.H. Kang, P. Wang, C. Qu, S. Shian, E.R. Chen, and K. Bertoldi, Harnessing multiple folding mechanisms in soft periodic structures for tunable control of elastic waves. Advanced Functional Materials 24 (2014) 4935-4942.

[3] D.R. Johnson, R.L. Harne, and K.W. Wang, A disturbance cancellation perspective on vibration control using a bistable snap-through attachment. Journal of Vibration and Acoustics 136 (2014) 031006.

[4] M.I. Hussein, M.J. Leamy, and M. Ruzzene, Dynamics of phononic materials and structures: historical origins, recent progress, and future outlook. Applied Mechanics Reviews 66 (2014) 040802.

[5] R.L. Harne, On the linear elastic, isotropic modeling of poroelastic distributed vibration absorbers at low frequencies. Journal of Sound and Vibration 332 (2013) 3646-3654.

[6] Z. Wu, R.L. Harne, and K.W. Wang, Energy harvester synthesis via coupled linear-bistable system with multistable dynamics. Journal of Applied Mechanics 81 (2014) 061005.

[7] D.A. Bies and C.H. Hansen, Engineering Noise Control: Theory and Practice, Spon Press, London, 2006.